Remote Sensing Applications: Society and Environment 32 (2023) 101055

Contents lists available at ScienceDirect

Remote Sensing Applications: Society and Environment

journal homepage: www.elsevier.com/locate/rsase

Assessing high resolution thermal monitoring of complex intertidal environments from space: The case of ECOSTRESS at Rias Baixas, NW Iberia

Nicolas Weidberg [a,b,*,1], Laura K. López Chiquillo [b], Salvador Román [b], Marta Román [b], Elsa Vázquez [b], Celia Olabarria [b], Sarah A. Woodin [a], David S. Wethey [a]

[a] Department of Biological Sciences, University of South Carolina, Columbia, SC, USA
[b] CIM – Centro de Investigación Mariña and Departamento de Ecoloxía e Bioloxía Animal, Facultade de Ciencias do Mar, Universidade de Vigo, Spain

ARTICLE INFO

Keywords:
ECOSTRESS
Calibration
Sandy mudflats
Fourier's law of heat conduction
Thermal stress
Shellfish beds

ABSTRACT

Currently, thermal sensors on satellites and other orbital platforms with high spatial resolution designed to monitor the oceans are often insufficient to assess the surface temperature of small bodies of water or within the coastal boundary layer. As the accuracy and sensitivity of remote sensing satellites improve, the demand for more accurate and up-to-date basic data sets for calibration increases. The quality of the thermal data collected by ECOSTRESS on the International Space Station allows the characterization of thermal stress levels in coastal ecosystems with a high spatial resolution of 70 m and a return time from hours to 5 days. This study focused on the calibration of ECOSTRESS estimates with *in situ* surface temperature data from sensors installed at 3 cm depth in the sediment on the intertidal muddy sandflats of three of the Rías Baixas in Galicia, NW Iberian Peninsula, from 2019 to 2021. A final number of 45 ECOSTRESS temperature images were analyzed. From these, 20% contained substantial georeferencing errors which had to be corrected manually with GIS software tools. We applied the Fourier's law of Heat Conduction to derive surface estimates from loggers sub-surface measurements that could be directly compared with ECOSTRESS data. Overall, a good calibration which explained more than 80% of ECOSTRESS temperature estimates for the whole dataset was obtained, but with an intrinsic cold bias around 1.39 °C. When temperatures at a depth of 3 cm were used, the linear fit became worse and the negative bias increased to 1.49 °C. Closer inspection revealed that night measurements were responsible for this larger deviation, as ECOSTRESS estimates became much colder compared to within sediment measurements because of the combined effect of the instrument intrinsic bias and nocturnal surface cooling. The best calibration was obtained when surface estimates were calculated just for the nighttime, as the cold bias decreased to 0.93 °C. More importantly, during hot daytime conditions in emersion above 20 °C, ECOSTRESS data matched surface temperature estimates, probably because of a better performance of ECOSTRESS algorithm at dry surfaces with lower emissivity. Thus, during the most ecologically relevant periods when high temperatures could drive thermal stress in many commercially-important bivalve species, ECOSTRESS provides accurate surface estimates that can be used to derive sub surface temperatures at the depths at

* Corresponding author. Department of Biological Sciences, University of South Carolina, Columbia, SC, USA.
E-mail address: weidbergnicolas@uniovi.es (N. Weidberg).
[1] Present address: Department of Organisms and Systems Biology; University of Oviedo, Spain.

https://doi.org/10.1016/j.rsase.2023.101055
Received 23 June 2023; Received in revised form 19 August 2023; Accepted 1 September 2023
Available online 4 September 2023

which the different burrowing organisms live. We thus conclude that this instrument constitutes an important global tool to examine thermal stress at an unprecedented spatial scale for complex sea-land boundary systems.

1. Introduction

Global warming has accelerated in recent years, with a 1.2 °C increase since pre-industrial times by 2020 and a projected increment of 3 °C by the end of this century according to most plausible scenarios (Geiges et al., 2020, IPCC, 2022). Due to complex atmospheric and oceanic circulation patterns, this warming is neither uniform in space nor in time, with extreme weather events becoming more frequent at certain regions (Moon et al., 2022; Rousi et al., 2022). Such events constitute perturbations that, depending on their magnitude and frequency, could alter ecosystem succession and overall functioning (Sanz-Lazaro 2016; Maxwell et al., 2019; Lugo 2020). From the perspective of the sustainability of human populations worldwide, the productivity of key ecoregions like coastal areas and temperate grasslands can be severely reduced if these systems reach critical tipping points at which they could shift to more unproductive stages (Bakun et al., 2015; Wu et al., 2021). Biodiversity losses can also occur, decreasing in turn the buffering effect that species richness can exert on potential public health risks like infectious diseases and the occurrence of biological invasions (Robinson et al., 2020; Baker et al., 2022; Mora et al., 2022). Sustainably managing ecosystems for their unique ecological and socio-economical functions requires a deep understanding of the main processes driving such changes. In this context, a proper high resolution characterization of thermal variability becomes crucial to determine the degree of change at multiple scales of biological organization, from individuals to ecosystems.

The NASA Ecosystem Spaceborne Thermal Radiometer Experiment on Space Station (ECOSTRESS) was designed to provide small spatial scale thermal monitoring on a global scale. It was installed on the International Space Station on June 29, 2018. Since then ECOSTRESS has retrieved more than 350,000 high resolution scenes with a pixel dimension of 70*70 m and a total size of approximately 400 × 400 km, globally between 52°N and 52°S with short revisiting times of hours to 5 days (Hook et al., 2020; Hulley et al., 2021; Weidberg et al., 2021). Skin temperatures for water, land and vegetation surfaces have been derived from brightness temperatures of 3 spectral bands since May 2019 (8.78, 10.49 and 12.09 μm) by using a temperature emissivity separation (TES) algorithm (Hook and Hulley, 2015). Overall, ECOSTRESS has been used to infer high spatial resolution thermal stress for crops, forests and human populations living in contrasting urban environments (Poulos et al., 2021; Richter et al., 2021; Li et al., 2022; Wu et al., 2022).

Calibrations with *in situ* sensors in the field and intercomparisons with other widely used orbital platforms have been carried out to assess the quality of ECOSTRESS temperature measurements. In short, negative biases around −1 °C occur for the ocean when ECOSTRESS extensive datasets were compared with the Visible Infrared Imaging Radiometer Suite VIIRS imagery (Weidberg et al., 2021). Consistently, similar nocturnal cold biases were obtained at buoys off the coasts of Florida (Shi and Hu, 2021). In general, for land surfaces this bias is greatly reduced, although negative deviations occur at nighttime when comparing with *in situ* sensors at usual NASA calibration sites (Hulley et al., 2021). Although easy to analyse and correct, the fact that these temperature biases change when comparing day vs night, sea vs land, and *in situ* calibrations *vs* orbital intercomparisons reveals that several sources of error may be behind such deviations.

The examination of ECOSTRESS measurements within complex environments with unique thermal and optical properties, like sea-land boundaries, becomes crucial to use this instrument as an effective global monitoring tool. Specifically, extensive soft sediment intertidal regions like muddy sandflats may be particularly difficult to characterise (Laignel et al., 2023). Sharp thermal contrasts are modulated by the daily entrainment of a thin layer of coastal waters with the high tide and the sediment desiccation driven by solar heating during low tide (Dyer et al., 2000; Befus et al., 2013). One such system is the Rias Baixas in the region of Galicia, which comprises a complex stretch of coastline formed by large estuaries at the NW corner of the Iberian Peninsula. Relatively cold and nutrient rich waters around 15 °C usually upwell at the open coast and entrain the rias, a process that happens all year round but is more persistent in spring/summer (Prego et al., 2007, Álvarez et al., 2009; Fernández et al., 2016). During daytime low tide aerial exposure, surface sediment temperatures can easily exceed 30 °C in summer, thus driving daily thermal contrasts of high magnitude (Leitao 2014; Domínguez et al., 2021; Román et al., 2022). The biological productivity of the Rias Baixas, especially at the intertidal muddy sandflats at their head end, sustains traditional coastal fisheries like those targeting several sedentary species such as bivalves (Fernández et al., 2016; Pascual-Fernández et al., 2020). Overall, more than 26,000 employments rely directly and indirectly on these coastal fisheries, which accounts for more than 60% of the total population working in the Galician fisheries (Villasante et al., 2021).

In summary, the Rias Baixas region offers a challenging case of study for an ECOSTRESS calibration due to its large spring/summer thermal contrasts on sub-daily time scales and its persistent cloud cover in autumn/winter. On the other hand, it also offers a unique opportunity to assess ECOSTRESS thermal monitoring potential in a region with key intertidal sandflats that sustain large populations of coastal organisms with a high socioeconomic importance. In this study, we carry out an ECOSTRESS calibration on a regional scale by using a set of temperature loggers placed at different intertidal muddy sandflats across Rias Baixas. Our goals were 1) to obtain representative, high quality ECOSTRESS imagery for the period 2019–2021 for this region; 2) to calibrate this dataset with *in situ* and concurrent temperature measurements; 3) to evaluate the potential of ECOSTRESS to characterise the thermal conditions for commercial bivalve species within the sediment; 4) to infer differences in ECOSTRESS performance based on contrasting thermal conditions on tidal, daily and seasonal time scales.

2. Material and methods

2.1. Temperature loggers

Temperature loggers were placed in intertidal shellfish beds within the 3 main rias covering the whole latitudinal thermal gradient that characterizes the Rias Baixas region (Fig. 1). From North to South, Testal in the Ría de Noia, O Sarrido in the Ría de Arousa, and A Seca in the Ría de Pontevedra were selected (Fig. 1, Table 1). These devices, which provided measurements with a temporal resolution of 30 min (EnvLogger version 2.4, https://electricblue.eu/), were placed in PVC frames called sticks that were firmly buried vertically in the sediment. Every stick was attached by a short rope to a 30 cm long PVC tube with a signaling buoy in order to avoid potential accidents with small boats at high tide. A logger was attached to every stick at a depth below the sediment surface of 3 cm. Six sticks were deployed at each of the 3 sites selected, 2 sticks at each of the 3 intertidal levels (low, middle and high, Fig. 1) from October 2019 to December 2021. However, temperature data were not available for the northern site in 2021 due to the loss of multiple sensors in the field.

2.2. ECOSTRESS images processing

A total of 104 ECOSTRESS images from 20 to 10–2019 to 5-12-2021 were retrieved from the NASA EarthData platform (Hook and Hulley, 2019) within a rectangular area comprising the NW Iberian coast (41°58′05.4"N 9°37′26.5"W - 43°25′24.1"N 8°00′24.6"W for the southwestern and northeastern corners, respectively). However, only 45 images were eventually selected for processing as the other 59 were discarded due to excessive cloud cover over the Rias Baixas region (Appendix A, Table 1). Specifically, geolocation (GEO), radiance (RAD), cloud mask (CLD) and temperature-emissivity (LSTE) files were downloaded for each image from the ECOSTRESS Land Surface Temperature and Emissivity Daily L2 Global 70m V001 collection. To reproject the images in UTM coordinates and visualise them in GIS software as GeoTIFFs, we used the ECOSTRESS_swath2grid.py script in Python (https://git.earthdata.nasa.gov/projects/LPDUR/repos/ecostress_swath2grid/browse). Then, temperature data were extracted for each individual image at the pixels corresponding to each logger location using the extraction tool in QGIS. Before data extraction, a total of 9 images had to be manually corrected due to geolocation problems by measuring the displacement distances from the coastline shapefile. These distances were always shorter than 5 km along the swath direction, mainly to the North East and South East (Appendix A Table 1).

2.3. Tidal height and day/night assignation

To perform separate ECOSTRESS calibrations for emersion and immersion conditions, we had to infer the logger absolute heights with respect to the lowest low water level for each location so they could be compared with the tidal height time series. Thus, we first identified the times at which each logger was first submerged by the incoming tide on 18, 19 and 20 April 2022 at O Sarrido, A Seca and Testal, respectively. Then, we associated each of these times with the time series of water heights measured at the closest tide gauge with a temporal resolution of 1 min for O Sarrido and A Seca, at distances of 15.5 and 4 km, respectively (http://www.iocsealevelmonitoring.org/station.php?code=vil2)), while the MOHID model was used for Testal as no nearby tide gauge within

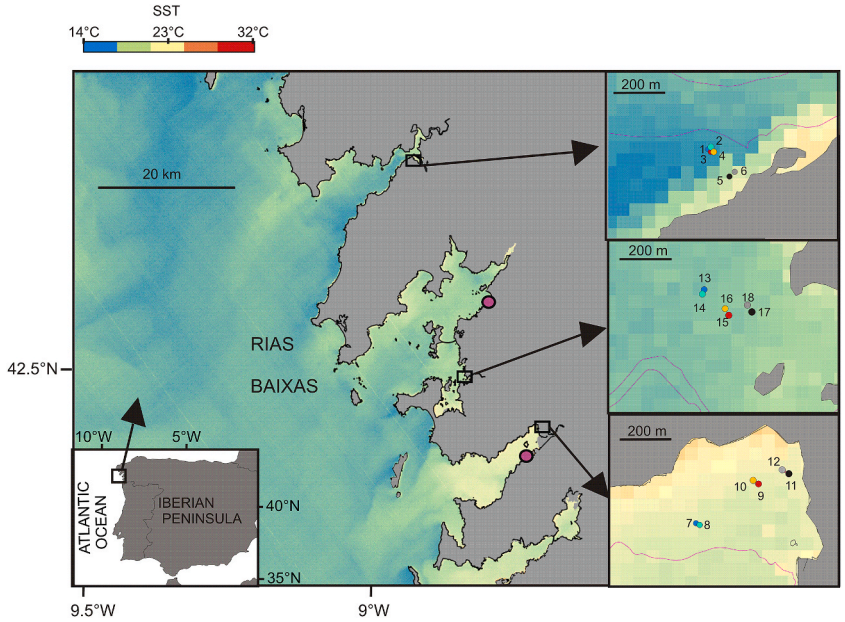

Fig. 1. Map of the study region. Purple points on the large panel show the location of the tide gauges at Vilagarcía (north) and Marin (south). Squares indicate sampling locations. On the small panels, bluish, orange/red and grey/black points represent the temperature loggers placed at low, mid and high intertidal positions, respectively. Numbers besides these points refer to the individual loggers whose characteristics are displayed in Table 1. (For interpretation of the references to colour in this figure legend, the reader is referred to the Web version of this article.)

Table 1
Temperature logger locations and tidal heights with respect to the lowest low water level.

Site	Logger	Latitude	Longitude	Height (m)
Testal	1	42°47′24.9"N	8°55′14.1"W	0.867
	2	42°47′24.9"N	8°55′14.1"W	0.867
	3	42°47′24.7"N	8°55′13.6"W	0.926
	4	42°47′24.7"N	8°55′13.6"W	0.926
	5	42°47′20.1"N	8°55′09.0"W	1.622
	6	42°47′20.9"N	8°55′08.1"W	1.622
O Sarrido	13	42°30′07.5"N	8°49′27.1"W	1.345
	14	42°30′07.2"N	8°49′27.3"W	1.345
	15	42°30′03.6"N	8°49′21.3"W	1.627
	16	42°30′04.2"N	8°49′22.0"W	1.568
	17	42°30′04.2"N	8°49′15.7"W	1.727
	18	42°30′04.9"N	8°49′16.9"W	1.727
A Seca	7	42°26′00.8"N	8°41′41.6"W	1.053
	8	42°26′00.8"N	8°41′41.2"W	1.053
	9	42°26′07.7"N	8°41′27.2"W	2.401
	10	42°26′08.1"N	8°41′28.3"W	2.317
	11	42°26′09.9"N	8°41′20.1"W	2.358
	12	42°26′10.1"N	8°41′20.7"W	2.256

the same ria was available. (http://mandeo.meteogalicia.es/thredds/catalogos/MOHID/catalog.html). MOHID is a 3D modelling system that incorporates the main physical process within the coastal ocean on different nested spatial scales (Neves, 1985; Martins, 1999). Then, MOHID data was regressed against heights at the closest tidal gauge to obtain an equation that allowed the calculation of heights right at Testal. The methodology is explained in greater detail in Román et al., (2023) *b*. Eventually, a height estimate was obtained for each sensor (Table 1) and compared with the corresponding water heights to assign the immersion or the emersion category for each time step. Given the quality and high spatiotemporal resolution of both MOHID and tide gauge measurements, we think that this method correctly splits the dataset in these two categories. Similarly, to perform separate calibrations for day and night periods, the sunpos and sunvector R functions (package insol, Corripio 2021) were applied to each GMT time step to assign the day/night condition to each individual measurement. Finally, the logger temperature time series were paired by time steps with ECOSTRESS temperatures using the R function data.table (Dowle and Srinivasan, 2021).

2.4. Surface correction

To derive surface temperatures that could be compared with ECOSTRESS skin temperatures from logger measurements at 3 cm, we applied Fourier's law of Heat Conduction, which establishes a relationship between temperatures at different depths as follows.

1) $TS = (AS^* (w^*t\text{-}zs/d)^*\exp(-z1/d) - AL^* (w^*t\text{-}zl/d)^*\exp(-zl/d)) + TL$

Where TS is surface temperature, TL is logger temperature, AS is amplitude of the daily temperature cycle at the surface, AL is amplitude of the daily temperature cycle at loggers' depth, w is 2π multiplied by the frequency of the temperature variation (24 h), zs is surface depth (we assume 0.1 cm), zl is logger depth (3 cm), d is damping depth (the depth at which the amplitude equals 1/e of AS), and t is time in seconds from sunrise calculated from the time at which each ECOSTRESS image was retrieved with the R package suncalc (Thieurmel and Elmarhraoui, 2022). We assumed a damping depth of 10.6 cm according to the measurements with sediments extracted from the same sites at Rias Baixas (Domínguez et al., 2021). Our vertical temperature profiles for stick 7 at A Seca with loggers at depths of 3, 8 and 13 cm also pointed to a damping depth around 10.6 cm. From Fourier's law we obtained daily sinusoidal patterns in temperature lagged in time and with a shorter amplitude as depth increases as a result of the vertical propagation of the heat waves within sediment layers. Time series of AL values were approximated as the difference between maximum and minimum daily temperatures divided by 2 and averaged across all loggers within a site. Then we calculated AS as follows.

2) $AS = (AL/(\exp(-zl/d)))^*\exp(-zs/10.6)$

This surface correction was applied to the whole dataset to compare ECOSTRESS skin temperature estimates with surface temperatures derived from logger data at 3 cm. On the other hand, we compared ECOSTRESS data with raw logger measurements at 3 cm to assess the potential of this orbital sensor to characterise within sediment temperatures. Then, to infer which data subsets showed the largest biases, the difference between ECOSTRESS and logger temperatures (ΔT) were plotted against time of the day for emersion and immersion. These patterns were all compared to the difference between TS and TL (ΔST) along a daily cycle calculated with mean daily amplitudes for all dates when ECOSTRESS images were retrieved. Thus, we could see if the temporal patterns in ECOSTRESS bias matched those caused by the deployment of loggers at 3 cm below sediment surface.

2.5. Statistical analyses

Linear regressions with logger temperature as the independent predictor and ECOSTRESS temperature as the dependent variable were performed for each of the 4 combinations between the immersion/emersion and day/night states. Temperature differentials consisting of subtracting logger temperatures from ECOSTRESS temperatures (ΔT) were also plotted against logger temperatures. To

assess the goodness of fit of these calibrations R^2, residual standard error (RSE), regression slope and mean ΔT estimates were obtained and evaluated. These procedures were carried out for surface temperatures derived from logger measurements; for raw logger data at 3 cm; and for the combination of both surface and 3 cm temperatures showing the best fits and smallest biases with respect to

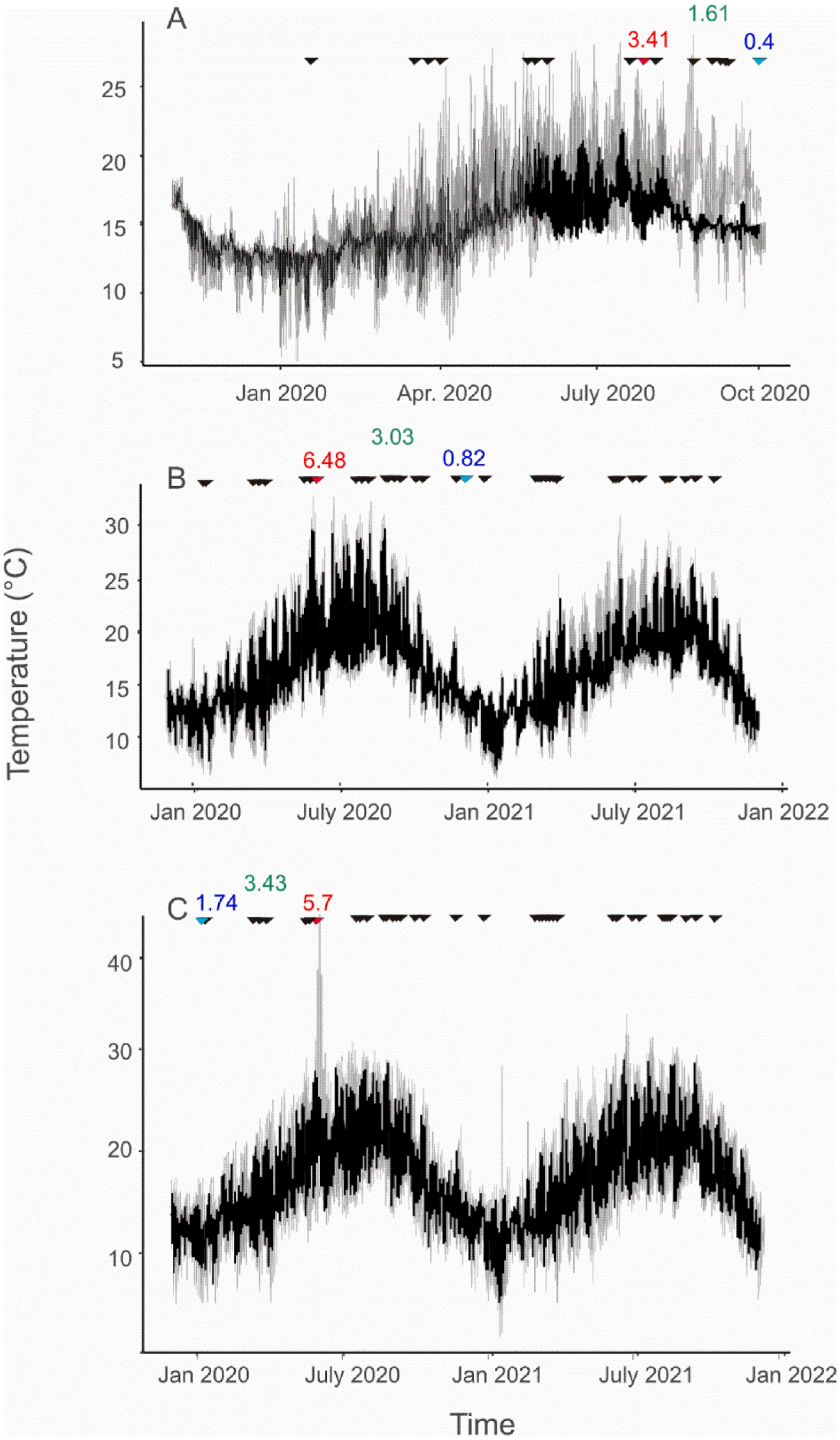

Fig. 2. Temperature time series from *in situ* loggers for A) Testal, B) O Sarrido and C) A Seca. Grey lines show the thermal envelope for each site taking into account all loggers, while the dark lines show mean temperatures for each time step across all loggers at each site. Inverted triangles show the dates at which ECOSTRESS scenes used for the calibration were retrieved. Red and blue triangles point to those retrieval dates showing maximum and minimum thermal amplitudes, respectively, for each site. Red and blue numbers show those values in °C, while mean amplitudes for all ECOSTRESS retrievals at each site are shown in green. (For interpretation of the references to colour in this figure legend, the reader is referred to the Web version of this article.)

ECOSTRESS.

In addition, to infer potential significant differences in ECOSTRESS calibrations due to the influence of tidal and light conditions, we followed the stepwise statistical procedure described in Engqvist (2005) and applied in Baldanzi et al. (2015) designed to disentangle the effects of covariates, factors and their interactions on a given target variable. First, a homogeneity of slopes model was performed with ECOSTRESS temperature as the dependent variable, surface temperature derived from logger measurements as the independent covariate and state with 4 levels (emersion and day; emersion and night; immersion and day; immersion and night) as factor. If the interaction between logger temperature and state was significant, then a separate slopes model was applied to analyse how temperature slopes change with state. If the interaction was not significant, then an analysis of covariance (ANCOVA) was carried out to assess properly the individual effect of logger temperature and state on ECOSTRESS temperature. Functions in the R packages *tidyverse, ggpubr, rstatix, lsmeans* and *broom* were used for these analyses (Lenth, 2016; Wickham et al., 2019; Kassambara, 2020, 2021; Robinson et al., 2022). These procedures were carried out for surface temperatures derived from logger measurements; for raw logger data at 3 cm; and for the combination of both surface and 3 cm temperatures showing the best fits and smallest biases with respect to ECOSTRESS.

3. Results

3.1. Logger temperature time series

Along the time series the seasonal thermal cycle typical of temperate regions was apparent, especially in O Sarrido and A Seca where two years of data were available. Although shorter, the time series for the northernmost site at Testal indicated a colder temperature regime, as sediment temperatures rarely exceeded 25 °C (Fig. 2A). Accordingly, minimum winter sediment temperatures in January 2020 of 5 °C were lower than those at the other two sites. Maximum sediment temperatures exceeding 40 °C were reached at the upper intertidal in A Seca between 25-5–2020 and 15-6-2020 (Fig. 2C). At O Sarrido, the summer of 2020 was warmer than summer 2021, reaching 33 °C compared to 30 °C in June 2021 (Fig. 2B).

The ECOSTRESS image dataset provided a good temporal coverage along the logger time series, although skewed towards the summer periods of 2020 and 2021 as expected due to the seasonal reduction in cloud cover (Fig. 2). Logger thermal amplitudes for the dates when ECOSTRESS scenes were obtained ranged between 0.4 °C at Testal to 6.48 °C at O Sarrido. Overall, much smaller thermal amplitudes were observed at the northernmost site of Testal (Fig. 2). Mean logger thermal amplitude across all sites was 2.93 °C, which resulted in a thermal amplitude of 3.85 °C at the surface with ECOSTRESS according to Fourier's law.

3.2. Daily variability of bias

Theoretical temperature differences between the surface calculated with the Fourier's law and loggers' depth at 3 cm followed a daily pattern with maximum and minimum values at midday and midnight, respectively, around 1.5 and −1.5 °C (Fig. 3A). This pattern arose because of the time lag in the diffusion of heat and the lower amplitude (2.93 °C versus 3.85 °C) of temperature time series at 3 cm compared to surface estimates.

ECOSTRESS imagery for the study area between 2019 and 2021 showed a good temporal coverage on sub-daily time scales (Fig. 3B). ΔT estimates in relation to time of the day followed LOESS fits, which peaked at midday and around 16:00 for the emersion

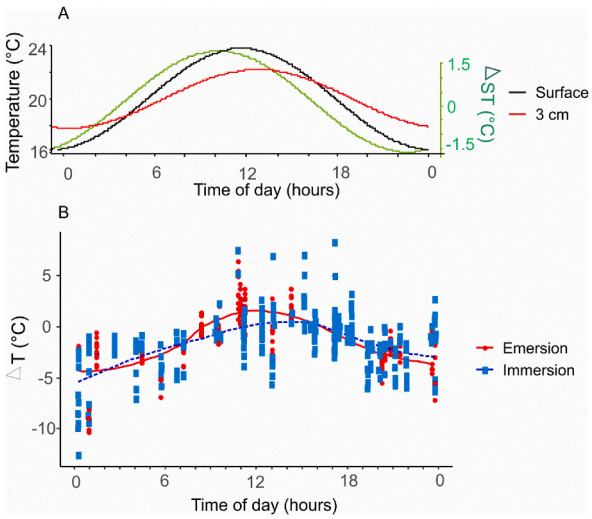

Fig. 3. A) Temperatures at the surface layer (0.1 cm, dark line) and at loggers' depth within the sediment (3 cm, red line) as a function of time of the day. The green line represents the surface – 3 cm thermal difference. These theoretical profiles were inferred from the Fourier's law with 20 °C as mean temperature and 3.85 and 2.93 °C as mean amplitudes for the surface and at a depth of 3 cm, respectively. These amplitudes were calculated across all sites for all ECOSTRESS retrieval dates. B) Thermal differentials between ECOSTRESS and loggers as a function of time of the day. Red and blue lines show LOESS fits for emersion and immersion, respectively. (For interpretation of the references to colour in this figure legend, the reader is referred to the Web version of this article.)

and immersion datasets, respectively, reaching almost zero bias values at those times. On the other hand, the largest average negative biases of approximately −5 °C was reached around midnight regardless of exposure to air.

Overall, the ECOSTRESS bias daily variability was consistent with that driven by loggers' position within the sediment as inferred from Fourier's law, as both follow a synchronised sinusoidal pattern. However, ΔT estimates were clearly skewed to lower values during the night, while Fourier's law temperature differences were symmetric around 0.

3.3. MOHID correction and loggers heights

We obtained a highly significant power law fit between water height measurements at the Vilagarcia tide station and MOHID water level forecasts with the following equation.

3) MOHID sea level height Testal = 0.5442 + 0.4001*(Tide gauge Vilagarcía $^{1.5104}$)

With $R^2 = 0.936$, (Appendix A Fig. 1, Román et al., 2023 *b*). Testal was found to be the site with the lowest heights, and A Seca presented the highest locations (Table 1).

3.4. Evaluation

The calibration between ECOSTRESS estimates and surface estimates derived from logger data presented a high R^2 above 80% and a negative bias of −1.39 °C (Table 2, Fig. 4). If the raw logger measurements were considered instead of the surface derived values, then biases increased to −1.49 °C and the goodness of fit decreased to 73.9% (Table 2, Figs. 4, Fig. 5). According to the regression line, this cold bias reversed when logger temperatures exceeded 25 °C (Fig. 5A). This temperature dependent bias switch was largely driven by the emersion-day dataset (Fig. 5E). The largest bias reduction (−0.93 °C) was obtained when the surface correction was only applied to nighttime data while keeping the 3 cm logger measurements for the daytime dataset. The goodness of fit of this last calibration remained above 80% (Table 2, Fig. 4 E, F).

Very good fits explaining greater than 70% of the variability were found when splitting the dataset into the 4 combinations of day-night and emersion-immersion conditions, especially for emersion during the day (Table 2). However, night calibrations exhibited a much larger cold bias of −3 °C compared with day calibrations that presented mean ΔTs between −0.3 and + 0.6 °C (Table 2). Negative biases were reduced from −3 °C to values around −2 °C when applying the surface correction for the nighttime subsets (Im & N, Em & N) (Table 2). Nighttime data in between 15 and 20 °C fell along the 1:1 line only when they were surface corrected, while they fell clearly below it when the correction was not applied (Fig. 5). On the other hand, negative biases appeared for the daytime subsets

Table 2
Calibrations for the whole dataset (all), emersion during the night (Em&N), emersion during the day (Em&D), immersion during the night (Im&N), and immersion during the day (Im&D). Variance explained (R^2), residual standard error (RSE) and mean temperature differentials (mean ΔT) are shown. Values in cursive stand for the calibrations performed with corrected surface temperatures following the Fourier's law. For the whole dataset, the values for the calibration with the nocturnal surface correction are shown in cursive, while those for the calibration with the overall surface correction are shown in red cursive.

	Estimate	Std. Error	t value	Pr(>|t|)	Significance	R2	RSE	Mean ΔT
Intercept	-5.57404	0.47314	-11.78	<2e-16	***			
	-4.04772	*0.39766*	*-10.18*	*<2e-16*	***			
	-2.77205	*0.37591*	*-7.374*	*5.73e-13*	***	0.739	2.597	-1.49
Temperature (all)	1.23068	0.02605	47.24	<2e-16	***	*0.826*	*2.38*	*-0.93*
	1.18174	*0.02249*	*52.55*	*<2e-16*	***			
	1.07850	*0.02062*	*52.304*	*<2e-16*	***	*0.824*	*2.39*	*-1.39*
Intercept	-3.685	1.176	-3.134	0.00274	**			
	-1.90585	*1.05729*	*-1.803*	*0.0768*	*n.s.*	0.791	2.087	-3.397
Temperature (Em&N)	1.017	0.069	14.744	< 2e-16	***			
	0.99834	*0.06761*	*14.767*	*< 2e-16*	***	*0.792*	*2.084*	*-1.93*
Intercept	-3.73736	0.9702	-3.852	0.000222	***	0.886	2.279	0.577
	-4.1641	*0.91810*	*-4.536*	*1.81e-05*	***			
Temperature (Em&D)	1.21086	0.04593	26.362	< 2e-16	***			
	1.13163	*0.03996*	*28.321*	*< 2e-16*	***	*0.9*	*2.137*	*-1.23*
Intercept	-5.65186	0.82404	-6.859	7.64E-11	***			
	-3.17855	*0.79354*	*-4.006*	*8.59e-05*	***	0.718	2.295	-3.148
Temperature (Im&N)	1.1536	0.04963	23.244	< 2e-16	***			
	1.07674	*0.05113*	*21.058*	*< 2e-16*	***	*0.677*	*2.459*	*-2.014*
Intercept	-1.19648	0.68198	-1.754	0.0807	n.s.			
	-0.08437	*0.75753*	*-0.111*	*0.911*	*n.s.*	0.787	2.075	-0.256
Temperature (Im&D)	1.0517	0.03672	28.64	<2e-16	***			
	0.96590	*0.03974*	*24.305*	*<2e-16*	***	*0.727*	*2.351*	*-0.72*

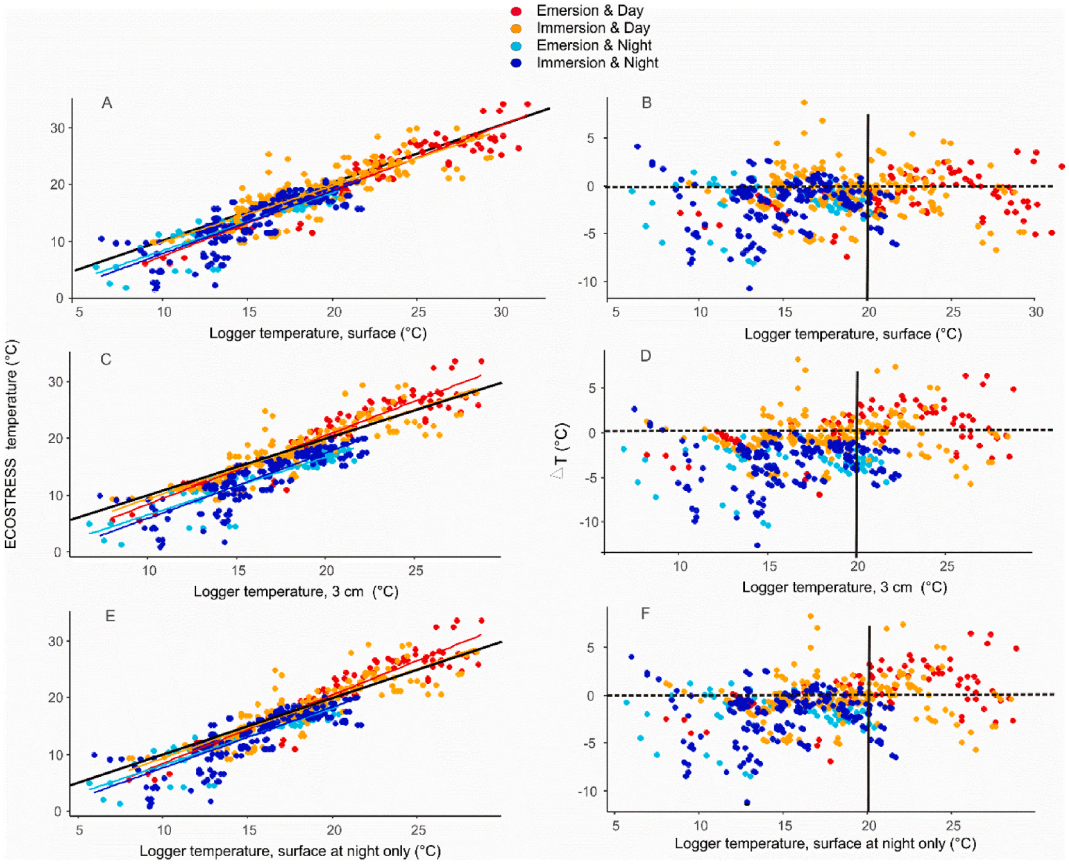

Fig. 4. Calibrations between logger and ECOSTRESS temperatures for the 4 states with their respective regression lines and the 1:1 line in black. Surface temperatures, logger temperatures at 3 cm and surface temperature only for nighttime were used in panels A, C and E, respectively. ECOSTRESS temperature differentials for the surface temperatures, for the logger temperatures at 3 cm and for surface temperature only for nighttime are shown in panels B, D and F, respectively. Horizontal dashed lines and vertical lines in panels B, D and F represent null thermal differentials and a logger temperature threshold of 20 °C, respectively.

when surface estimates were used, especially in emersion (from +0.6 °C to −1.23 °C, Table 2). Nevertheless, surface estimates for extreme warm conditions within the emersion-daytime dataset above 20 °C fell closer to the 1:1 line. The goodness of fit remained almost the same after applying the surface correction for each subset (Table 2).

Individual ΔT values clearly differed between day and night, with negative values during the night for both emersion and immersion conditions and more positive values, although close to 0, during much of the day (Fig. 4B, D, F, Fig. 5D, F). The somewhat positive bias (+0.6 °C) occurred during the daytime in emersion as expected. On the other hand, nighttime negative biases were reduced and were closer to 0 when surface temperatures were used (Fig. 4B and F), while daytime biases became more negative (Fig. 4B).

Regarding the homogeneity of slopes model, it revealed a significant state: temperature interaction, thus pointing to a shift in slope depending on light conditions and air exposure (Table 3). The separate slopes model with the interaction as the unique source of variation yielded the same result (Table 3). These results held when surface corrections were applied to the whole dataset or just to the nighttime subsets (Table 3). Pairwise slope comparisons showed that within the day and the night datasets, the slopes did not change significantly between immersion and emersion (Table 4, Figure 4). However, between the day and night datasets, slopes were always different regardless of the emersion/immersion condition (Table 4, Fig. 4). The same pattern was observed when surface estimates were used just for the nighttime subsets (Table 4). However, when the surface correction was applied to the whole dataset, day-night differences in slope for emersion disappeared. Also, differences in slope between the emersion & daytime and the immersion & nighttime subsets became non-significant (Table 4).

4. Discussion

4.1. Cloud cover limitations and geolocation errors

ECOSTRESS provides a thermal characterization of both land surfaces and water bodies within the infrared band with the highest spatial resolution available at the moment (70*70m, Fisher et al., 2020). Thus, ECOSTRESS imagery can be used to determine coastal thermal patterns at regions that cannot be properly characterised by usual oceanographic satellites (Weidberg et al., 2021). In this study, we show that ECOSTRESS can be very useful in areas like the Rias Baixas region (NW Iberian Peninsula), where the intricate

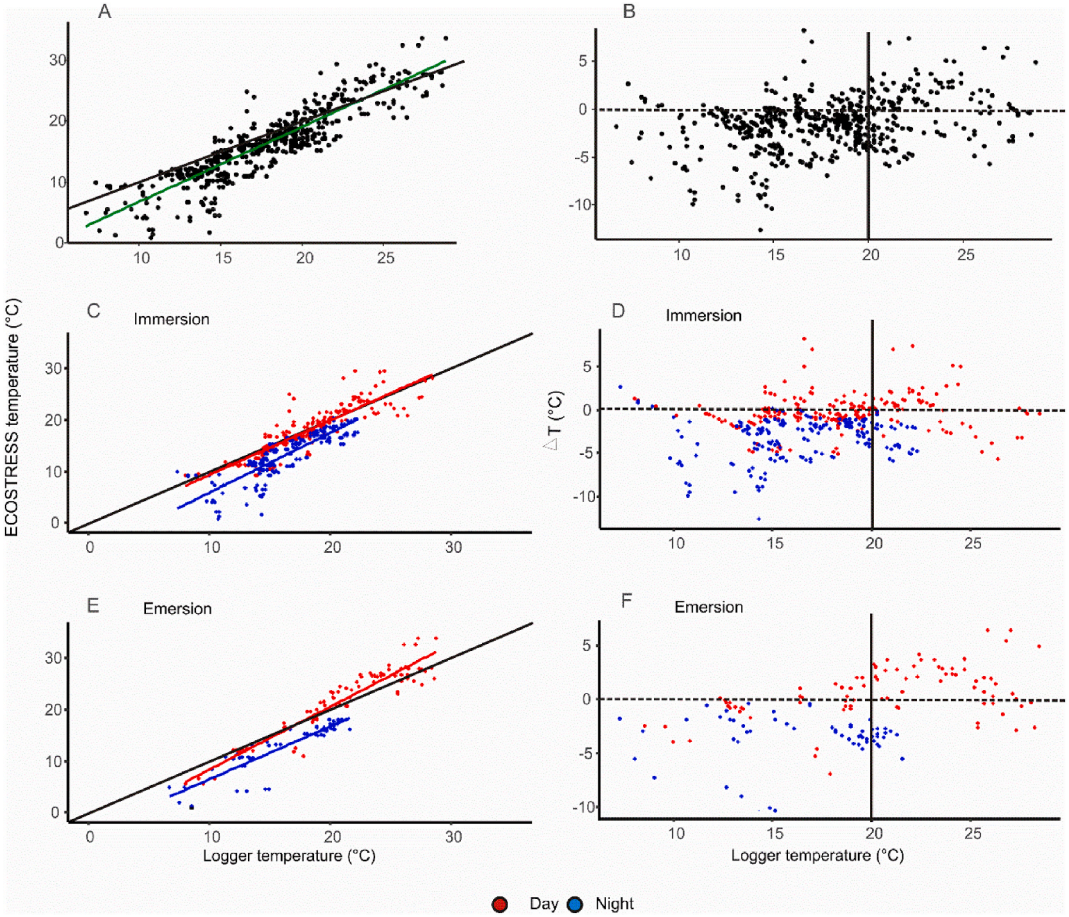

Fig. 5. Calibrations between logger and ECOSTRESS temperatures. Raw temperatures (A, C, E) and thermal differentials (B, D, F) are shown for the whole dataset (A, B), immersion (C, D) and emersion (E, F). Red and blue lines show linear regression fits for day and night, respectively, while the 1:1 line is shown in black. Horizontal dashed lines and vertical lines in panels B, D and F represent null thermal differentials and a logger temperature threshold of 20 °C, respectively. (For interpretation of the references to colour in this figure legend, the reader is referred to the Web version of this article.)

coastal topography with extensive shallow areas driven by extreme tidal forcing supposes a severe limitation for other observational orbital platforms. However, given its geographical location right within the eastward track of Atlantic low pressure systems (Naranjo and Perez-Muñuzuri 2006), persistent cloud cover above Rias Baixas was the main factor limiting the number of images available for analysis, with more than 42% of ECOSTRESS scenes discarded for this reason.

Additionally, there were evident geolocation errors in 20% of the images. Shi and Hu (2021) found similar geographic displacements that were corrected with the use of Landsat base-maps and geometric corrections based on topographic landmarks. Most likely, these inaccuracies are due to the intrinsic uncertainties of the ISS orbit with frequent changes in altitude (Fisher et al., 2020) and human activity inside the station. Also, geolocation depends upon a fixed reference land-water boundary, yet in Galicia there are large tidal flats, so the land-water boundary changes by km depend upon the state of the tide unless identifiable rocky headlands are used exclusively for geolocation. In addition, the fact that the image displacement direction matches the ISS swath direction (Northwest to Southeast, or Southwest to Northeast, Appendix A Table 1) points to a delay in processing and acquiring the image as a potential source of the error, a problem already described in previous high resolution sensors on the ISS (Dou et al., 2013). Geolocation errors can also appear in satellite imagery like in the Cross-track Infrared Sounder (CrIS) mounted on the Suomi National Polar-orbiting Partnership (SNPP) platform. In this case, changing geolocation parameters in time are the source of displacement errors in the order of few kms (up to 4.7 km, Gong et al., 2018), that are substantially larger than those we have observed with ECOSTRESS. Nevertheless, such errors can be easily mitigated with automatic and simplified correction procedures (Wang et al., 2017).

4.2. *Surface calibration*

Overall, ECOSTRESS measurements presented a negative bias of −1.39 °C with respect to surface estimates derived from *in situ* temperature loggers at Rias Baixas (Table 2, Fig. 3). This result is in agreement with previous global calibrations like the intercomparison performed against N20-VIIRS SST data at different seas all over the world, which yielded a −1.01 °C bias (Weidberg et al., 2021). The source of the bias was attributed to the limitations of the ECOSTRESS TES algorithm to derive temperatures from emissivity

Table 3
Results for the homogeneity and separate slopes models. The values for the analyses with the nocturnal surface correction are shown in cursive, while those for the analyses with the overall surface correction are shown in red cursive.

Analysis	Effect	DFn	DFd	F	p	Significance
Homogeneity of slopes model	State	3	574	77.063 *21.327* *8.447*	6.72E-42 *4.14E-13* *1.68e-05*	*** *** ***
	Temperature	1	574	2268.64 *2109.15* *1926.613*	1.45E-201 *2.29E-194* *1.40e-185*	*** *** ***
	State:Temperature	3	574	3.281 *3.191* *2.919*	0.02 *0.023* *0.034*	* * *
Separates slopes model	State:Temperature	4	577	819.034 *783.686* *709.343*	3.04E-236 *1.46E-231* *4.17e-221*	*** *** ***

Table 4
Post-hoc contrasts for the slopes across all states. The values for the analyses with the nocturnal surface correction are shown in cursive, while those for the analyses with the overall surface correction are shown in red cursive.

Contrast	Estimate	SE	df	t.ratio	p.value
Em&N vs Em&D	-0.1944 *-0.11965* *-0.03326*	0.0209 *0.0231* *0.0241*	577	-9.279 *-5.182* *-1.378*	<.0001 *<.0001* *0.5139*
Em&N vs Im&N	-0.0194 *0.00107* *0.00144*	0.0194 *0.0215* *0.0224*	577	-0.997 *0.050* *0.065*	0.751 *1* *0.999*
Em&N vs Im&D	-0.1668 *-0.0857* *-0.05848*	0.019 *0.021* *0.0219*	577	-8.789 *-4.078* *-2.665*	<.0001 *0.0003* *0.0395*
Em&D vs Im&N	0.175 *0.12071* *0.0347*	0.0155 *0.0167* *0.0176*	577	11.287 *7.213* *1.972*	<.0001 *<.0001* *0.197*
Em&D vs Im&D	0.0276 *0.03394* *-0.02522*	0.014 *0.0142* *0.0142*	577	1.971 *2.386* *-1.775*	0.2001 *0.0809* *0.2865*
Im&N vs Im&D	-0.1474 *-0.08677* *-0.05993*	0.0125 *0.0136* *0.0143*	577	-11.79 *-6.366* *-4.195*	<.0001 *<.0001* *0.0002*

estimates that were too low and inaccurate for graybodies with high emissivity like water and vegetation (Weidberg et al., 2021). In fact, the global calibration performed by Hulley et al. (2021) with *in situ* radiometer measurements and modelled estimates in both water and land surfaces yielded similar results. They estimated a cold bias of −0.75 °C that was slightly larger at night (around −1 °C). We observed similar but larger negative temperature differentials with logger corrected surface temperatures during nighttime (around −2 °C, Table 2).

4.3. Nighttime effects

On top of the cold bias due to the performance of the ECOSTRESS TES algorithm, we found clear evidences of temperature deviations due to the mismatch between measurements of skin temperatures and the ones we collected with our loggers at depths of 3 cm within the sediment. The combined effect of the algorithm related bias and the deviations derived from heat propagation effects within the sediment resulted in a greater negative bias for the night than for day when the raw temperature measurements of the loggers at depths of 3 cm were used for the calibration (Table 2, Figs. 4, Fig. 5). This pattern occurs because the negative algorithm intrinsic bias adds on to surface cooling during the night. Thus, when we applied the surface correction just for the nighttime subsets, then the overall goodness of fit increased and the bias decreased (Table 2, Figs. 4, Fig. 5).

In agreement with this mismatch caused by the position of the loggers, we observed that the daily pattern of variability in ΔT mirrored the temperature differences expected by Fourier's law, with a surface cooling with respect to temperatures within the sediment at midnight (Fig. 3). Similarly, negative SST deviations were found mainly during the night between ECOSTRESS and bulk measurements at 2 m depth off the coast of southern Florida and they were attributed to nighttime surface cooling (Shi and Hu, 2021). These effects are compensated during the day as a thermocline usually develops due to surface heating (Minnett, 2003). Note that the calibrations, including this study, with *in situ* sensors measuring bulk temperatures rather than skin temperatures show a much marked nighttime negative bias whether in water or in intertidal surfaces (Shi and Hu, 2021), while the intercomparison with VIIRS N-20 does not (Weidberg et al., 2021). Most likely, the lack of this marked nighttime negative bias shows that both orbital platforms are capturing the nocturnal surface cooling within the skin layer. In fact, data retrieval and processing for VIIRS N-20 incorporates a specific split window nighttime algorithm (Minnett et al., 2020).

4.4. Daytime effects

Conversely, the combination of both the intrinsic ECOSTRESS negative bias and the heat propagation effects within the sediment resulted in a smaller negative bias for the day when logger raw temperature measurements were considered (Table 2, Figs. 4, Fig. 5). This pattern occurs because the negative algorithm intrinsic bias compensates surface overheating during the day and, consequently, brings surface estimates closer to cooler temperatures 3 cm within the sediment. Thus, when the surface correction was applied to the whole dataset, surface daytime temperatures increased because of overheating and therefore a negative bias with respect to colder ECOSTRESS estimates affected by the algorithm limitations appeared (Table 2, Figs. 4, Fig. 5). In other words, because of their intrinsic cold bias, ECOSTRESS measurements were a better predictor of temperatures at 3 cm within the sediment than at the surface in daytime, although this rule may not hold during extreme hot conditions in emersion.

4.5. Emersion vs immersion

Our calibrations showed that, within the daytime and nighttime categories, the immersion and emersion datasets presented similar negatives biases, RSE and slopes (Table 2, Table 4, Figs. 4, Fig. 5). Although a priori land surfaces present very different optical and thermal properties, in the case of intertidal sand flats such as those of the inner part of Rias Baixas such differences could be masked by the nature of their sediment and vegetation. Overall, wet sediments and vegetation could blur the differences in surface emissivity between emersion and immersion. The size spectrum of the sediment grains in these systems is modulated by riverine and tidal currents, bathymetric profile and wave dynamics (Méndez and Vilas, 2005). In the inner part of the Rias Baixas very fine muddy sediments with high water content prevail (Vilas, 2002). In addition, our temperature logger sites were located within or very close to meadows of the seagrass *Zostera noltei* (Hornemann, 1832), an intertidal species common along the southern and western European coasts (Green and Short 2003). Moreover, the larger subtidal species *Zostera marina* (Linnaeus 1753) with wider and longer leaves was present in the intertidal of O Sarrido (personal observations). These plants favour the retention of water and suspended particles (Wilkie et al., 2012). Besides, vegetation presents a very high emissivity around 0.99, which matches that of water (Rubio et al., 1997). Thus, the thermal properties of the surfaces where temperatures were retrieved by ECOSTRESS might not be expected to change between emersion and immersion.

Nevertheless, when loggers registered temperatures higher than 20 °C during emersion in daytime, ECOSTRESS biases became positive (Fig. 4D, F, Fig. 5). Most of these measurements corresponded to summertime dry sediment conditions, when *Z. noltei* water content decreases, especially during pervasive heat waves, and sediment water content reaches its minimum (Allen 1987; Zipperle et al., 2009). Thus, for these particular measurements the negative intrinsic algorithm bias may not apply as surface emissivity may be lower and in turn the TES algorithm performance should be better. Consistently, the smallest biases quite close to 0 have been found in extremely dry, hot regions like the Gobabel desert (Hulley et al., 2021). Therefore, positive biases with respect to temperatures within the sediment caused by surface overheating are no longer compensated by the intrinsic ECOSTRESS negative bias for these hot summer daytime emersion periods. Accordingly, when the surface correction was used for the emersion-daytime data, measurements above 20 °C were better aligned with the 1:1 line, while the slope of the linear regression decreased and became more similar to the trends of the other subsets (Figure. 4A, B, Table 4).

4.6. Consequences for ecological monitoring in shellfish beds

Along the inner parts of Rias Baixas, several bivalve species of commercial interest inhabit the muddy and sandy intertidal sediments, including the native clams *Ruditapes decussatus* (Linnaeus 1758), *Venerupis corrugata* (Gmelin 1791), the introduced *Ruditapes philippinarum* (Adams and Reeve, 1850), and the cockle *Cerastoderma edule* (Linnaeus 1758) (Fernández et al., 2016; Pascual-Fernández et al., 2020). Their fishery brings in 50 million € per year in first sales (https://www.pescadegalicia.gal/gl/estatisticas). These species display different ranges of thermal tolerance and burrowing behaviours in response to summertime heatwaves (Domínguez et al., 2021). On one end of the spectrum, *V. corrugata* with their narrower thermal range and cockles with their limited ability to burrow (up to 2 cm), are more affected by thermal stress. On the other end of the spectrum, the introduced *R. philippinarum*, with a much wider thermal range, and *R. decussatus*, that can burrow up to depths of 13 cm in the sediment, are more able to resist increased thermal stress (Verdelhos et al., 2015; Macho et al., 2016; Domínguez et al., 2021; Román et al., 2022, 2023 *a*).

Another coastal shellfisheries with extensive intertidal flats subjected to thermal stress that can be potentially monitored with ECOSTRESS are that of the European oyster *Ostrea edulis* (Linnaeus 1758) and the Pacific oyster *Magallana gigas* (Thunberg 1793) along the Atlantic coasts of France. In fact, oyster leases in Arcachon Bay are of the same spatial scale than ECOSTRESS pixels, thus allowing a proper individual thermal characterization of every management unit in this fishery (Wethey et al., 2022). Although oysters can apparently resist and perform well up to air temperatures of 30 °C (Dutertre et al., 2010; Eymann et al., 2020) even when they belong to epifauna, high temperatures are known to drive pervasive diseases in *M. gigas* that in turn have led to large mortality events (Goulletquer et al., 1998). In general, the effects of increased temperatures on intertidal bivalves do not scale linearly from the individual to the population level, which complicates predictions on their biological fitness in the mesoscale (Thomas and Bacher, 2018). Nevertheless, warming trends forced by anthropogenic greenhouse effects along European coasts of around 0.025 °C/year (Lima and Wethey, 2012; Varela et al., 2022) can potentially affect even the more resistant species (Castro-Olivares et al., 2022). In particular, atmospheric heat waves over Western Europe have increased in number and magnitude triggered by the anomalous jet stream circulation forced by global warming (Rousi et al., 2022).

4.7. Conclusions

To correctly use ECOSTRESS for the characterization of thermal stress for these shellfish species, we have to consider the calibrations performed for those data subsets that overpassed critical warm temperatures beyond 20 °C or even 30 °C. Thus, nighttime calibrations with their large negative bias are of little importance for ecological monitoring at these habitats. On the other hand, daytime calibrations, specifically in emersion, are critical as they reach those thermal thresholds (Figs. 4 and 5). Then, as the bias reached its minimum around 0.5 °C in daytime during emersion when temperatures at 3 cm within the sediment were used (Table 2), we could infer that ECOSTRESS provides reliable, straightforward temperature measurements at the habitat depth of many soft bottom intertidal species within the subsurface layer. However, specifically for those critical measurements above 20 °C, the positive bias with respect to loggers at depths of 3 cm became much larger (Fig. 4D,F, Fig. 5F), probably because of a reduction of surface emissivity of dryer, less vegetated surfaces during emersion in summertime that is translated to a better performance of the TES algorithm. Therefore, for these periods of high thermal stress, we recommend to use ECOSTRESS datasets as a good proxy of surface temperatures. Then, these temperatures can be used directly to evaluate thermal stress for those species inhabiting the surface like oysters, or they can be used to derive within sediment temperatures at those depths where different clam species live by applying Fourier's law. Used properly, ECOSTRESS becomes a very valuable tool to appropriately track the occurrence of heat wave episodes and extreme hot summers over large coastal areas with high spatial resolution for different shellfish species.

CRediT author statement

Nicolas Weidberg: Methodology, Conceptualization, Formal analysis, Data Curation, Investigation, Writing-original draft, Supervision, Visualization. Laura K. López Chiquillo: Data Curation, Formal Analysis, Investigation, Writing-original draft, Visualization. Salvador Román: Data Curation, Methodology, Investigation, Writing-review and editing. Marta Román: Writing-review and editing, Visualization. Elsa Vázquez: Writing-review and editing, Supervision, Funding Acquisition. Celia Olabarria: Writing-review and editing, Supervision, Funding Acquisition. Sarah A. Woodin: Methodology, Conceptualization, Formal analysis, Investigation, Writing-review and editing, Supervision, Visualization, Funding Acquisition. David S. Wethey: Methodology, Conceptualization, Formal analysis, Investigation, Writing-review and editing, Supervision, Visualization, Funding Acquisition.

Funding

This research was supported by NASA project "ECOSTRESS – heat and desiccation risk prediction in intertidal shellfisheries" (80NSSC20K0074), the ZEUS project (RTI2018-095583-B-I00) from the Spanish Ministerio de Ciencia e Innovación/Agencia Estatal de Investigación and by the Autonomous government Xunta de Galicia-FEDER (ED431C 2021/42): "ERDF A way of making Europe". Salvador Román was supported by a PhD fellowship from the Xunta de Galicia (ED481A-2020/199).

Ethical statement

Here I declare that all ethical practices have been followed in relation to the development, writing, and publication of the article we are submitting. Best regards.

Nicolas Weidberg, 23-06-2023.

Declaration of competing interest

The authors declare that they have no known competing financial interests or personal relationships that could have appeared to influence the work reported in this paper.

Data availability

Data will be made available on request.

Acknowledgements

We thank Andrés Simón, José Carlos Mariño and Liliana Pérez technical assistants of the Cofradías de Pescadores of Campelo, Cambados and Noia respectively for their assistance with the fieldwork.

Appendix A. Supplementary data

Supplementary data to this article can be found online at https://doi.org/10.1016/j.rsase.2023.101055.

References

Allen, J.R.L., 1987. Desiccation of mud in the temperate intertidal zone: studies from the Severn Estuary and Eastern England. Philos. Trans. R. Soc. B. 315 (1171), 127–156. http://www.jstor.org/stable/2396522.

Álvarez, I., Ospina-Álvarez, N., Pazos, Y., deCastro, M., Bernárdez, P., Campos, M.J., Gómez-Gesteira, J.L., Álvarez-Ossorio, M.T., Varela, M., Gómez-Gesteira, M., 2009. A winter upwelling event in the northern Galician Rias: frequency and oceanographic implications. Estuar. Coast Shelf Sci. 82, 573–582.

Baker, R.E., Mahmud, A.S., Miller, I.F., Rajeev, M., Rasambainarivo, F., Rice, B.L., Takahashi, S., Tatem, A.J., Wagner, C.E., Wang, L.-F., Wesolowski, A., Metcalf, C.J. E., 2022. Infectious disease in an era of global change. Nat. Rev. Microbiol. 20, 193–205. https://doi.org/10.1038/s41579-021-00639-z.

Bakun, A., Black, B.A., Bograd, S.J., García-Reyes, M., Miller, A.J., Rykaczewski, R.R., Sydeman, W.J., 2015. Anticipated effects of climate change on coastal upwelling ecosystems. Curr. Clim. Change Rep. 1, 85–93. https://doi.org/10.1007/s40641-015-0008-4.

Baldanzi, S., Weidberg, N., Fusi, M., Cannicci, S., McQuaid, C.D., Porri, F., 2015. Contrasting environments shape thermal physiology across the spatial range of the sandhopper. Talorchestia capensis. https://doi.org/10.1007/s00442-015-3404-5.

Befus, K.M., Cardenas, M.B., Erler, D.V., Santos, I.R., Eyre, B.D., 2013. Heat transport dynamics at a sandy intertidal zone. Water Resour. Res. 49, 3770–3786. https://doi.org/10.1002/wrcr.20325.

Castro-Olivares, A., Des, M., Olabarria, C., deCastro, M., Vázquez, E., Sousa, M.C., Gómez-Gesteira, M., 2022. Does global warming threaten small-scale bivalve fisheries in NW Spain? Mar. Environ. Res. 180, 105707 https://doi.org/10.1016/j.marenvres.2022.105707.

Corripio, J.G., 2021. _insol: solar Radiation_. R package version 1.2.2. https://CRAN.R-project.org/package=insol.

Domínguez, R., Olabarria, C., Woodin, S.A., Wethey, D., Peteiro, L.G., Macho, G., Vázquez, E., 2021. Contrasting responsiveness of four ecologically and economically important bivalves to simulated heat waves. Mar. Environ. Res. 164, 105229 https://doi.org/10.1016/j.marenvres.2020.105229.

Dou, C., Zhang, X., Kim, H., Ranganathan, J., Olsen, D., Guo, H., 2013. Geolocation algorithm for earth observation sensors onboard the international space station. PE&RS. 79 (7), 625–637. https://doi.org/10.14358/pers.79.7.625.

Dowle, M., Srinivasan, A., 2021. _data.table: extension of 'data.frame'_. R package version 1.14.2. https://CRAN.R-project.org/package=data.table.

Dutertre, M., Beninger, P.G., Barillé, L., Papin, M., Haure, J., 2010. Rising water temperatures, reproduction and recruitment of an invasive oyster, Crassostrea gigas, on the French Atlantic coast. Mar. Environ. Res. 69 (1), 1–9. https://doi.org/10.1016/j.marenvres.2009.07.002.

Dyer, K.R., Christie, M.C., Wright, E.W., 2000. The classification of intertidal mudflats. Continent. Shelf Res. 20, 1039–1060.

Engqvist, L., 2005. The mistreatment of covariate interaction terms in linear model analyses of behavioural and evolutionary ecology studies. Anim. Behav. 70, 967–971.

Eymann, C., Götze, S., Bock, C., Guderley, H., Knoll, A.H., Lannig, G., Sokolova, I.M., Aberhan, M., Pörtner, H.O., 2020. Thermal performance of the European flat oyster, Ostrea edulis (Linnaeus, 1758)—explaining ecological findings under climate change. Mar. Biol. 167 (17) https://doi.org/10.1007/s00227-019-3620-3.

Fernández, E., Álvarez-Salgado, X.Á., Beiras, R., Ovejero, A., Martínez, G., 2016. Coexistence of urban uses and shellfish production in an upwelling-driven, highly productive marine environment: the case of the Ría de Vigo (Galicia, Spain). Region. Stud. Mar. Sci. 8, 362–370. https://doi.org/10.1016/j.rsma.2016.04.002.

Fisher, J.B., Lee, B., Purdy, A.J., Halverson, G.H., Dohlen, M.B., Cawse-Nicholson, K., Wang, A., Anderson, R.G., Aragon, B., Arain, M.A., et al., 2020. ECOSTRESS: NASA's next generation mission to measure evapotranspiration from the international space station. Water Resour. Res. 56 (4).

Geiges, A., Nauels, A., Yanguas Parra, P., Andrijevic, M., Hare, W., Pfleiderer, P., Schaeffer, M., Scheleussner, C.F., 2020. Incremental improvements of 2030 targets insufficient to achieve the Paris Agreement goals. Earth Syst. Dynam. 11, 697–708. https://doi.org/10.5194/esd-11-697-2020.

Gong, X., Li, Z., Li, J., Moeller, C.C., Cao, C., Wang, W., Menzel, W.P., 2018. Intercomparison between VIIRS and CrIS by taking into account the CrIS subpixel cloudiness and viewing geometry. J. Geophys. Res. Atmos. 123 https://doi.org/10.1029/2017JD027849.

Goulletquer, P., Soletchnik, P., Le Moine, O., Razet, D., Geairon, P., Faury, N., Taillade, S., 1998. Summer Mortality of the Pacific Cupped Oyster Crassostrea gigas in the Bay of Marennes-Oléron (France). ICES STATIJTORY MEETING 1998. Mariculture Committee CM 1998/CC: 14. Theme Session (CC): Population Biology.

Green, E.P., Short, F.T., 2003. World Atlas of Seagrasses, first ed. University of California Press, Berkeley.

Hook, S.J., Hulley, G.C., 2015. Level 2 Land Surface Temperature and Emissivity Algorithm Theoretical Basis Document (ATBD). 599 NASA JPL Report. https://ecostress.jpl.nasa.gov/downloads/atbd/ECOSTRESS_L2_ATBD_LSTE_2018-03-08.pdf.

Hook, S., Hulley, G., 2019. ECOSTRESS land surface temperature and emissivity daily L2 global 70 m V001. https://doi.org/10.5067/ECOSTRESS/ECO2LSTE.001.

Hook, S.J., Cawse-Nicholson, K., Barsi, J., Radocinski, R., Hulley, G.C., Johnson, W.R., Rivera, G., Markham, B., 2020. In-flight validation of the ECOSTRESS, Landsats 7 and 8 thermal infrared spectral channels using the Lake Tahoe CA/NV and Salton Sea CA automated validation sites. IEEE Trans. Geosci. Rem. Sens. 58, 1294–1302. https://doi.org/10.1109/TGRS.2019.2945701.

Hulley, G.C., Gottsche, F.M., Rivera, G., Hook, S.J., Freepartner, R.J., Martin, M.A., Cawse-Nicholson, K., Johnson, W.R., 2021. Validation and quality assessment of the ECOSTRESS Level-2 land surface temperature and emissivity product. IEEE Trans. Geosci. Rem. Sens. 60, 1–23. https://doi.org/10.1109/TGRS.2021.3079879.

IPCC, 2022. In: Pörtner, H.-O., Roberts, D.C., Tignor, M., Poloczanska, E.S., Mintenbeck, K., Alegría, A., Craig, M., Langsdorf, S., Löschke, S., Möller, V., Okem, A., Rama, B. (Eds.), Climate Change 2022: Impacts, Adaptation, and Vulnerability. Contribution of Working Group II to the Sixth Assessment Report of the Intergovernmental Panel on Climate Change. Cambridge University Press, Cambridge, UK and New York, NY, USA, p. 3056. https://doi.org/10.1017/9781009325844. Cambridge University Press.

Kassambara, A., 2020. _ggpubr: 'ggplot2' Based Publication Ready Plots_. R package version 0.4.0. https://CRAN.R-project.org/package=ggpubr.

Kassambara, A., 2021. _rstatix: pipe-friendly framework for basic statistical tests_. R package version 0.7.0. https://CRAN.R-project.org/package=rstatix.

Laignel, B., Vignudelli, S., Almar, R., Becker, M., Bentamy, A., Benveniste, J., Birol, F., Frappart, F., Idier, D., Salameh, E., et al., 2023. Observation of the coastal areas, estuaries and deltas from space. Surv. Geophys. https://doi.org/10.1007/s10712-022-09757-6.
Leitao, P., 2014. MOHID implementation in parallel mode following a domain decomposition approach to the Rias Baixas area, pp. 1–20. Technical Report.
Lenth, R., 2016. Least-squares means: the R package lsmeans. J. Stat. Software 69 (1), 1–33. https://doi.org/10.18637/jss.v069.i01.
Li, D., Newman, G.D., Wilson, B., Zhang, Y., Brown, R.D., 2022. Modeling the relationships between historical redlining, urban heat, and heat-related emergency department visits: an examination of 11 Texas cities. Environ. Plan. B Urban Anal. City Sci. 49 (3), 933–952. https://doi.org/10.1177/23998083211039854.
Lima, F.P., Wethey, D.S., 2012. Three decades of high-resolution coastal sea surface temperatures reveal more than warming. Nat. Commun. 3, 704. https://doi.org/10.1038/ncomms1713.
Lugo, A.E., 2020. Effects of Extreme Disturbance Events: from ecesis to social–ecological–technological systems. Ecosystems 23, 1726–1747.
Macho, G., Woodin, S.A., Wethey, D.S., Vázquez, E., 2016. Impacts of sublethal and lethal high temperatures on clams exploited in European fisheries. J. Shellfish Res. 35, 405–419.
Martins, F.A., 1999. Modelação matemática tridimensional de escoamentos costeiros e estuarinos usando uma abordagem de coordenada vertical genérica. PhD thesis. Technical University of Lisbon, Portugal.
Maxwell, S.L., Butt, N., Maron, M., McAlpine, C.A., Chapman, S., Ullmann, A., Segan, D.B., Watson, J.E., 2019. Conservation implications of ecological responses to extreme weather and climate events. Divers. Distrib. 25, 613–625.
Méndez, G., Vilas, F., 2005. Geological antecedents of the rias Baixas (Galicia, northwest iberian Peninsula). J. Mar. Syst. 54, 195–207.
Minnett, P.J., 2003. Radiometric measurements of the sea-surface skin temperature: the competing roles of the diurnal thermocline and the cool skin. Int.J. Remote Sens 24, 5033–5047. https://doi.org/10.1080/0143116031000095880.
Minnett, P.J., Kilpatrick, K.A., Podestá, G.P., Evans, R.H., Szczodrak, M.D., Izaguirre, M.A., Williams, E.J., Walsh, S., Reynolds, R.M., Bailey, S.W., et al., 2020. Skin sea-surface temperature from VIIRS on Suomi-NPP—NASA continuity retrievals. Rem. Sens. 12 (3369) https://doi.org/10.3390/rs12203369.
Moon, W., Kim, B.M., Yang, G.H., Wettlaufer, J.S., 2022. Wavier jet streams driven by zonally asymmetric surface thermal forcing. Proc. Natl. Acad. Sci. USA 119 (38).
Mora, C., McKenzie, T., Gaw, I.M., Dean, J.M., von Hammerstein, H., Knudson, T.A., Setter, R.O., Smith, C.Z., Webster, K.M., Patz, J.A., et al., 2022. Over half of known human pathogenic diseases can be aggravated by climate change. Nat. Clim. Change 12, 869–875. https://doi.org/10.1038/s41558-022-01426.
Naranjo, L., Perez Muñuzuri, V., 2006. A variabilidade natural do clima en Galicia, first ed. Xunta de Galicia.
Neves, R.J.A., 1985. Bidimensional model for residual circulation in coastal zones. Application to the Sado Estuary. Ann. Geophys. 3 (4), 465–472.
Pascual-Fernández, J., Florido del Corral, D., De la Cruz Modino, R., Villasante, S., 2020. Small-scale fisheries in Spain: challenges and prospects. In: Pascual-Fernández, J., Pita, C., Bavinck, M. (Eds.), Small-scale Fisheries in Europe: Status, Resilience and Governance. Springer, Switzerland, pp. 253–282.
Poulos, H.M., Barton, A.M., Koch, G.W., Kolb, T.E., Thode, A.E., 2021. Wildfire severity and vegetation recovery drive post-fire evapotranspiration in a southwestern pineoak forest, Arizona, USA. Remote Sens. Ecol. Conserv. 7 (4), 579–591.
Prego, R., Guzman-Zuniga, D., Varela, M., deCastro, M., Gomez-Gesteira, M., 2007. Consequences of winter upwelling events on biogeochemical and phytoplankton patterns in a western Galician ria (NW Iberian Peninsula). Estuar. Coast Shelf Sci. 73, 409–422.
Richter, R., Hutengs, C., Wirth, C., Bannehr, L., Vohland, M., 2021. Detecting tree species effects on forest canopy temperatures with thermal remote sensing: the role of spatial resolution. Rem. Sens. 13, 135. https://doi.org/10.3390/rs13010135.
Robinson, T.B., Martin, N., Loureiro, T.G., Matikinca, P., Robertson, M.P., 2020. Double trouble: the implications of climate change for biological invasions. NeoBiota 62, 463–487. https://doi.org/10.3897/neobiota.62.55729.
Robinson, D., Hayes, A., Couch, S., 2022. _broom: convert statistical objects into tidy tibbles_. R package version 0.8.0. https://CRAN.R-project.org/package=broom.
Román, M., Gilbert, F., Viejo, R.M., Román, S., Troncoso, J.S., Vázquez, E., Olabarria, C., 2023. Are clam-seagrass interactions affected by heatwaves during emersion? Mar. Environ. Res. 186, 105906.
Román, S., Vázquez, E., Román, M., Viejo, R.M., Woodin, S.A., Wethey, D.S., Troncoso, J.S., Olabarria, C., 2022. Effects of warming on biological interactions between clams and the seagrass *Zostera noltei*: a case study using open top chambers. Estuar. Coast Shelf Sci. 276, 108027 https://doi.org/10.1016/j.ecss.2022.108027.
Román, S., Olabarria, C., Weidberg, N., Román, M., Vázquez, E., 2023. Population structure and habitat assessment for two commercial clam species exploited in small scale fisheries. Rev. Fish Biol. Fish. https://doi.org/10.1007/s11160-023-09791-6.
Rousi, E., Kornhuber, K., Beovide-Arsuaga, G., Luo, F., Coumou, D., 2022. Accelerated western European heatwave trends linked to more-persistent double jets over Eurasia. Nat. Commun. 13 (3851).
Rubio, E., Caselles, V., Badenas, C., 1997. Emissivity measurements of several soils and vegetation types. Remote Sens. Environ. 59, 490–521.
Sanz-Lazaro, C., 2016. Climate extremes can drive biological assemblages to early successional stages compared to several mild disturbances. Sci. Rep. 6, 30607.
Shi, J., Hu, C., 2021. Evaluation of ECOSTRESS thermal data over South Florida estuaries. Sensors 21, 4341. https://doi.org/10.3390/s21134341.
Thieurmel, B., Elmarhraoui, A., 2022. _suncalc: Compute Sun Position, Sunlight Phases, Moon Position and Lunar Phase_. R Package Version 0.5.1.
Thomas, Y., Bacher, C., 2018. Assessing the sensitivity of bivalve populations to global warming using an individual-based modelling approach. Global Change Biol. 24 (10), 4581–4597. https://doi.org/10.1111/gcb.14402.
Varela, R., Rodríguez-Díaz, L., de Castro, M., Gómez-Gesteira, M., 2022. Influence of Canary upwelling system on coastal SST warming along the 21st century using CMIP6 GCMs. Global Planet. Change 208, 103692. https://doi.org/10.1016/j.gloplacha.2021.103692.
Verdelhos, T., Marques, J.C., Anastácio, P., 2015. Behavioral and mortality responses of the bivalves Scrobicularia plana and Cerastoderma edule to temperature, as indicator of climate change's potential impacts. Ecol. Indicat. 58, 95–103. https://doi.org/10.1016/j.ecolind.2015.05.042.
Vilas, F., 2002. Rias and tidal-sea estuaries. In: Encyclopedia of Life Support Systems. UNESCO-EOLSS. UNESCO, Paris.
Villasante, S., Tubío, A., Gianelli, I., Pita, P., García-Allut, A., 2021. Ever changing times: sustainability transformations of Galician small-scale fisheries. Front. Mar. Sci. 8, 712819 https://doi.org/10.3389/fmars.2021.712819.
Wang, L., Zhang, B., Tremblay, D., Han, Y., 2017. Improved scheme for cross-track infrared sounder geolocation assessment and optimization. J. Geophys. Res. Atmos. 122, 519–536. https://doi.org/10.1002/2016JD025812.
Weidberg, N., Wethey, D.S., Woodin, S.A., 2021. Global intercomparison of hyper-resolution ECOSTRESS temperature measurements from the Space Station with VIIRSN20. Rem. Sens. 13 (24), 5021.
Wethey, D.S., Weidberg, N., Woodin, S.A., 2022. Validation and use of the new high resolution NASA ECOSTRESS instrument in highly valuable harvested intertidal environments. Ocean Sci. Meet. Online, 24 February - 4 March. OSM web site.
Wickham, H., Averick, M., Bryan, J., Chang, M., McGowan, L.D., Francois, R., Grolemund, G., Hayes, A., Henry, L., Hester, J., et al., 2019. Welcome to the tidyverse. J. Open Source Softw. 4 (43), 1686. https://doi.org/10.21105/joss.01686.
Wilkie, L., O'Hare, M.T., Davidson, I., Dudley, B., Paterson, D.M., 2012. Particle trapping and retention by *Zostera noltii*: a flume and field study. Aquat. Bot. 102, 15–22.
Wu, G.L., Cheng, Z., Alatalo, J.M., Zhao, J., Liu, Y., 2021. Climate warming consistently reduces grassland ecosystem productivity. Earth's Future 9, e2020EF001837. https://doi.org/10.1029/2020EF001837.
Wu, J., Feng, Y., Liang, L., He, X., Zeng, Z., 2022. Assessing evapotranspiration observed from ECOSTRESS using flux measurements in agroecosystems. Agric. Water Manag. 261, 107706.
Zipperle, A.M., Coyer, J.A., Reise, K., Gitz, E., Stam, W.T., Olsen, J.L., 2009. Clonal architecture in an intertidal bed of the dwarf eelgrass *Zostera noltii* in the Northern Wadden Sea: persistence through extreme physical perturbation and the importance of a seed bank. Mar. Biol. 156 (10), 2139–2148. https://doi.org/10.1007/s00227-009-1244-8.